JOURNAL OF Materials CHEMISTRY

Surface structures and defect properties of pure and doped La_2NiO_4

Mark S. D. Read,[a]† M. Saiful Islam,*[a] Graeme W. Watson[b] and Fred E. Hancock[c]

[a]*Department of Chemistry, University of Surrey, Guildford, UK GU2 7XH. Fax: (01483) 876851; Tel: (01483) 876850; E-mail: m.islam@surrey.ac.uk*
[b]*Department of Chemistry, Trinity College, Dublin 2, Ireland*
[c]*Synetix, P.O. Box 1, Billingham, Cleveland, UK TS23 1LB*

Received 22nd March 2001, Accepted 22nd June 2001
First published as an Advance Article on the web 7th August 2001

Computer modelling techniques are used to investigate the surface properties and defect chemistry of the La_2NiO_4 material. Relaxed surface structures and energies are calculated for the low index planes which are used to predict the equilibrium crystal morphology. The {111} surface is calculated to dominate in the absence of impurities, water or surface irregularities, with significant contributions from the {100} and {001} surfaces. Isovalent doping of the Ni site by Fe and Cu is found to affect the crystal morphology by increasing the expression of the {001} surface, although Fe doping is predicted to create the {011} face which is not present in the undoped crystal. The Sr dopant at the La site is calculated to be the most soluble of the alkaline earth metals, in accord with observation. Charge compensation is predicted to occur *via* the formation of Ni(III), which is consistent with bulk calculations and catalytic models in which Ni(III) species are correlated to the observed catalytic activity.

Introduction

Ceramic oxides based on La_2NiO_4 with the perovskite-like K_2NiF_4 structure have been widely studied for their catalytic properties (*e.g.* partial oxidation,[1–9] hypochlorite decomposition[10]), and their electrical behaviour[11–14] in relation to the isostructural La_2CuO_4 superconductor. This includes investigations of the evolution of the electronic and magnetic structure with the mixed valence Ni(II)/Ni(III) states. More recently, the Sr-doped system, $La_{2-x}Sr_xNiO_{4+\delta}$, has generated considerable interest as a candidate mixed conductor[15–18] for use in solid oxide fuel cells (SOFCs) and in ceramic oxygen generators. Much of this attention is due to the favourable ionic–electronic conduction and surface oxygen exchange properties in comparison to the acceptor-doped $LaMO_3$ perovskites (where M = Mn, Co,Fe).

It is clear that surface properties such as the precise surface structures and the role of point defects and dopants are crucial to the proper understanding of the catalytic and electrochemical properties.[19] These aspects are also of importance for further insight as to the properties of nanoparticles. However, limited attention has been paid to the structure and defect redox chemistry of the La_2NiO_4 surfaces, due in part to the difficulties concerned with obtaining high-quality experimental data for mixed-metal oxide surfaces at the atomic level. It is now well established that computer modelling techniques[20,21] have made widespread contributions to the study of defect, ion transport and surface properties of a wide variety of oxide compounds, including catalysts[22–25] and perovskite-type conductors.[26,27]

Our previous simulation studies of La_2NiO_4 have concentrated on bulk properties.[28] These simulations predict that the interstitial oxygen position in oxygen-rich $La_2NiO_{4+\delta}$ is between adjacent LaO layers (in accord with neutron diffraction data), and that Fe doping enhances Ni(III) hole formation whereas Cu doping depresses such formation. More recently, Minervini *et al.*[29] have used simulation techniques to examine excess oxygen accommodation and migration in $La_2NiO_{4+\delta}$. Here we extend the scope of our earlier study by focusing on the structures and point defects at the surfaces of La_2NiO_4. This includes an examination of the crystal morphology using surface energetics, and the effect of dopant substitution at both cation sublattices.

Simulation techniques

The simulations presented here use the same methodology for the treatment of surfaces as employed in previous studies of oxide materials (*e.g.* $MgAl_2O_4$,[30] La_2O_3,[24] CeO_2–ZrO_2,[31] $LaCoO_3$ [32]), and are embodied within the METADISE[22] code. Since these techniques have been discussed in detail in earlier reviews,[21,28] only the main aspects for the treatment of surfaces will be outlined here.

The simulations are formulated within the Born model of ionic solids, in which the long-range terms are evaluated for the surface simulations by a "plane-by-plane" summation due to Parry.[33,34] Because of the two-dimensional periodicity of the surface calculation, we eliminate the need for large voids between blocks which is required in the alternate slab methodology. The Coulombic interaction is supplemented with a Buckingham potential to account for the short-range repulsion between neighbouring electron charge clouds and the van der Waals attraction. Ionic polarisability is described by means of the shell model and found to be crucial for reliable defect calculations.

The oxide surface is not considered simply as a termination of the bulk lattice. The structure (and energy) of a surface are obtained by relaxing the ions to their mechanical equilibrium positions. This was achieved *via* a two region approach in which the ion coordinates in the surface region are adjusted so that they experience zero net force, whilst those ions which are distant from the surface ("bulk region") are kept fixed at their equilibrium positions.

The energy (γ_i) of a particular surface is calculated from the difference between the surface block (E_{surf}) and the same

†Current address: AWE, Aldermaston, Reading, Berkshire, UK RG7 4PR.

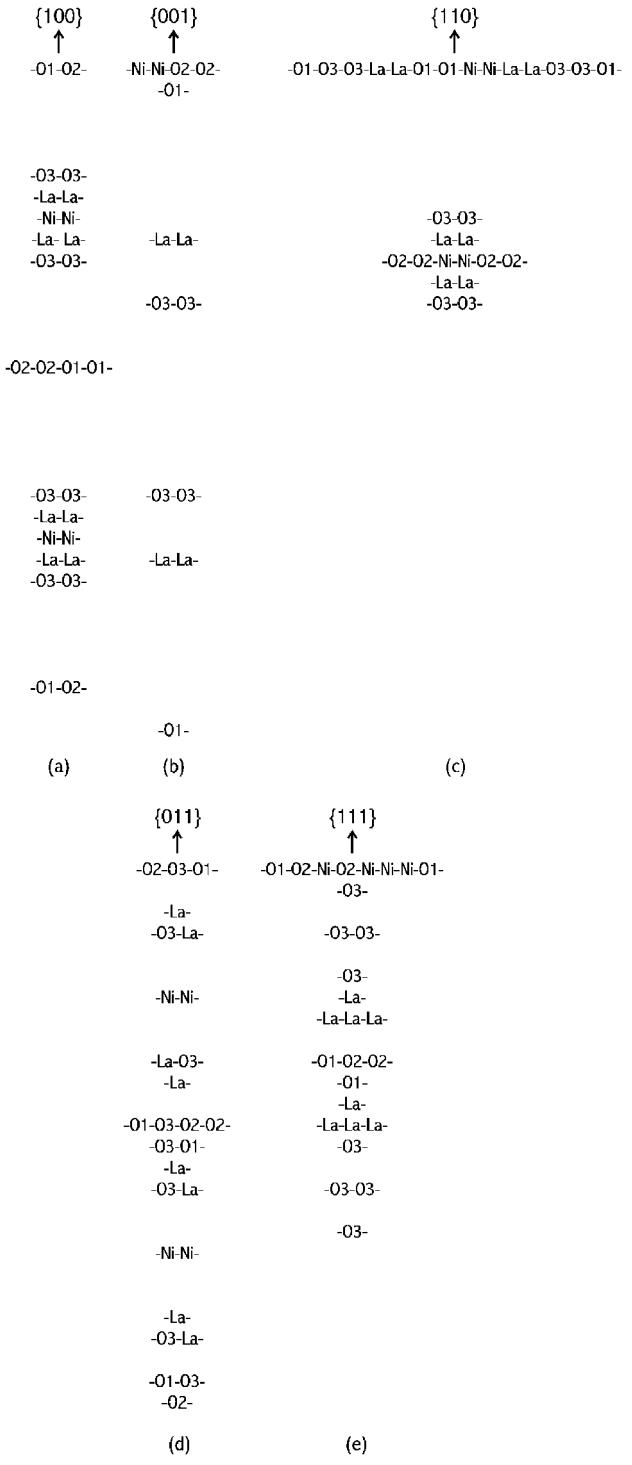

Fig. 1 Schematic representation of the stacking sequences for the low-index surfaces of La_2NiO_4, where O1 and O2 are equatorial oxygens and O3 apical oxygens.

number of bulk ions (E_{bulk}) per unit area, given by eqn. (1) (A = area):

$$\gamma_i = \left(\frac{E_{surf} - E_{bulk}}{A}\right) \quad (1)$$

However, the calculated Coulombic energy is divergent if there is a dipole in the repeat cell perpendicular to the pure surface.[35] As a consequence, Tasker[36] identified three types of surface cell or repeat unit. In Type I surfaces the surface cell is composed of single planes containing both cations and anions in a stoichiometric ratio and hence there can be no dipole perpendicular to the surface. Type II cells are composed of a number of distinct charge planes but are arranged such that the repeat cell has no dipole perpendicular to the surface. Type III surfaces are composed of alternately charged planes that produce a dipole perpendicular to the surface if the crystal is cut between any adjacent planes of atoms.

The crystal morphology can be predicted from the surface energies using Wulff's theorem.[37] This is related to the earlier theorem of Gibbs[38] who proposed that the equilibrium form of a crystal should possess minimal total surface energy for a given volume. The crystal morphology is derived from a polar plot of surface energy as a function of orientation. This is only valid for crystals grown with all faces in equilibrium and does not take account of kinetic factors such as growth rate. For small crystals where rearrangement of the crystal at each stage of the growth process is possible a morphology close to the equilibrium form would be expected.

Results and discussion

Surface energies and crystal morphology of La_2NiO_4

The K_2NiF_4-type structure of La_2NiO_4 consists of perovskite units (of NiO_6 octahedra) alternating with LaO rock-salt layers. The potential parameters used in this study are those employed in our previous simulations of La_2NiO_4, which correctly reproduce the observed structure to within 0.5% of the lattice parameters and to within 0.08 Å of the bond lengths.[28] It is evident that to augment the various redox processes in the bulk of the material, a knowledge of the surface structure is required. However, limited attention has been paid to the structure and defect chemistry of the La_2NiO_4 surfaces.

Several low index planes were first examined and their surface energies calculated for each respective non-dipolar termination using a sufficiently large region size to ensure convergence of the surface energy and structure. The study was subsequently reduced to five low index surfaces due to the tetragonal symmetry of the La_2NiO_4 unit cell, namely {100}, {001}, {110}, {011} and {111}. The stacking sequences of the most stable non-dipolar 'cuts' of these surfaces are shown in Fig. 1. The calculated unrelaxed and relaxed surface energies for the five surfaces considered are listed in Table 1.

Considerable relaxation occurs (up to 68% reduction in energy) suggesting that the relaxation of ions in the surface region can significantly increase the stability of that surface. In general, the perturbation of the structure at oxide surfaces is considerably more pronounced than in metals. It is found that La_2NiO_4 is similar to Nd_2CuO_4,[39] α-Al_2O_3 and α-Fe_2O_3[40] in that lattice relaxation changes the relative stability of the lowest-index surfaces. This in itself is an important result, as discussions on catalytic behaviour based on ideal surfaces may be incorrect. Although the surface energies are similar (Table 1), it is clearly seen that the order of stability for the relaxed surfaces of undoped La_2NiO_4 is: {100} > {111} > {110} > {001} > {011}.

Experimental surface energies, which are difficult to measure, are unavailable for La_2NiO_4. Nevertheless, the energies presented here are in the range obtained from similar simulation work on the isostructural La_2CuO_4,[39,41] although only the {100} and {001} surfaces were examined. Extensive relaxation at both surfaces of the cuprate leading to similar

Table 1 Calculated surface energies of La_2NiO_4

	Surface energy/J m^{-2}	
Miller index	Unrelaxed	Relaxed
100	3.07	0.98
001	3.55	1.55
110	3.82	1.45
011	4.48	1.69
111	3.19	1.08

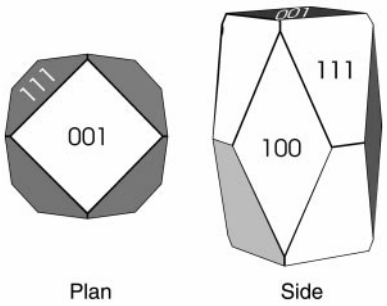

Fig. 2 Calculated crystal morphology of La_2NiO_4 (plan and side views) from the relaxed surface energies.

surface energies was predicted, indicating that the two faces would be important for inter-granular superconductivity.[39]

Direct comparison of surface energies with experiment is not always possible due to the lack of reliable data, but crystal morphology is one indirect measure which can be predicted from the surface energies. The simulation approach has been applied successfully to the prediction of crystal morphologies of inorganic solids such as calcite,[42] silica sodalite,[23] α-Cr_2O_3 and ZnO.[43] Recent work[30,44,45] has also demonstrated the value of these techniques in the investigation of the specific modification of crystal morphology in the presence of additives, a process of importance to a wide variety of technological processes.

The results from the morphology calculation on pure La_2NiO_4 are shown in Fig. 2 as schematic representations of the predicted single crystal.

Examination of the results shows that the {111} face will dominate the low-temperature crystal morphology in the absence of dopants, water or surface irregularities, with significant expressions of the {100} and {001} surfaces. The crystal is anisotropic with a tetragonal-like habit capped by {001}. Unfortunately there are limited single-crystal experiments for direct comparison, although Jang and Takei[46] have grown single crystals of $La_{2-x}Sr_xNiO_4$ which reveal facets of (001). The results therefore suggest that the {111}, {100} and {001} surfaces are expected to play an important role in catalysis and electrochemistry. It should be stressed that the oxygen-excess material $La_2NiO_{4+\delta}$ (where $\delta>0$) is not considered here. Nevertheless, our results will be of relevance to recent work on the oxygen-rich system which has potential use in solid oxide fuel cells and ceramic oxygen generators.

Surface structures of La_2NiO_4

Crystal surfaces are often imagined to be perfect, planar terminations of the bulk crystal structure. However, even for flat, defect-free planar terraces the equilibrium surface structure is usually modified from that of the bulk. Ionic oxides tend to exhibit significant relaxation which usually manifests in the form of either rumpling, (*i.e.* differential relaxation of cations and anions at the surface) or a net relaxation of the interplanar spacing in the surface region. The unrelaxed (top view) and relaxed (side view) structures of each of the five low-index planes of La_2NiO_4 are shown in Figs. 3–7 and discussed in the following subsections.

{100} Surface

Fig. 1(a) and Fig. 3 indicate how this surface is terminated with oxygen ions. Fig. 3 shows that the Ni–O_{ax} bonds of NiO_6 octahedra lying on the outermost plane are distorted parallel to the surface, accompanied by La and certain equatorial oxygen ions moving upwards away from the bulk by up to $\sim$1 Å. These relaxations cause a sinusoidal displacement of Ni in the Ni–O_{eq} plane perpendicular to the surface. These relaxations occur in the lower layers and diminish until negligible

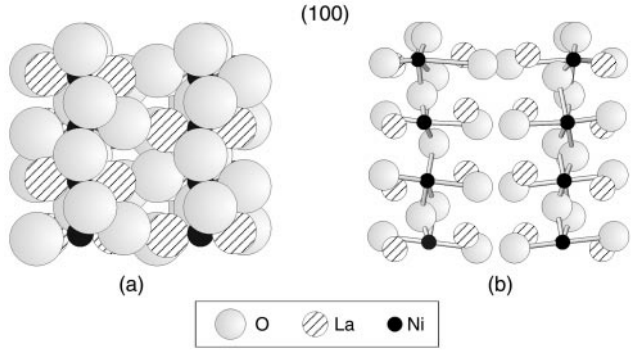

Fig. 3 Surface structures for the {100} surface of La_2NiO_4: (a) unrelaxed (top view), (b) relaxed (side view). For clarity, the top and side views are shown with full and half scale ion radii, respectively.

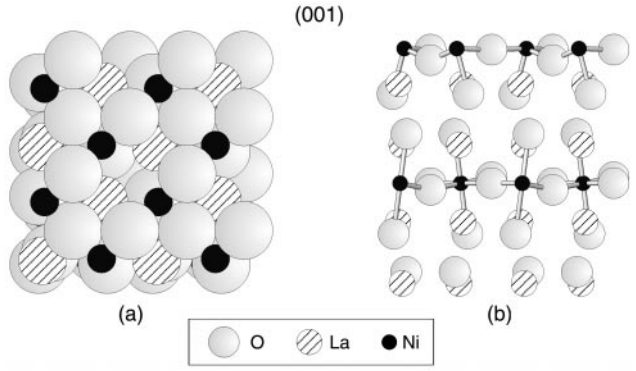

Fig. 4 Surface structures for the {001} surface of La_2NiO_4: (a) unrelaxed (top view), (b) relaxed (side view). For clarity, the top and side views are shown with full and half scale ion radii, respectively.

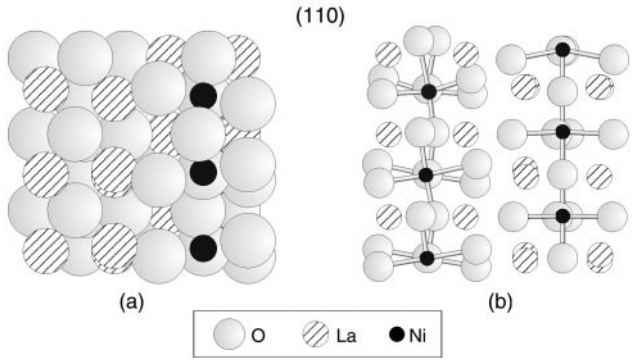

Fig. 5 Surface structures for the {110} surface of La_2NiO_4: (a) unrelaxed (top view), (b) relaxed (side view). For clarity, the top and side views are shown with full and half scale ion radii, respectively.

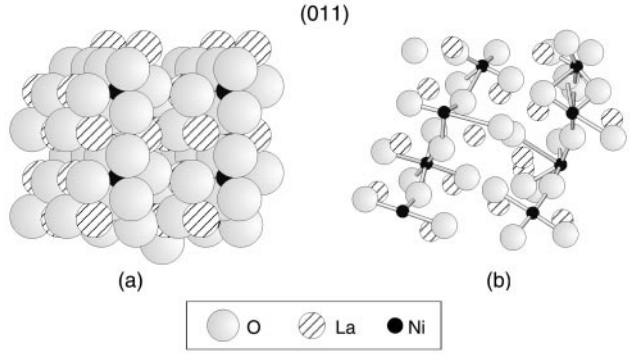

Fig. 6 Surface structures for the {011} surface of La_2NiO_4: (a) unrelaxed (top view), (b) relaxed (side view). For clarity, the top and side views are shown with full and half scale ion radii, respectively.

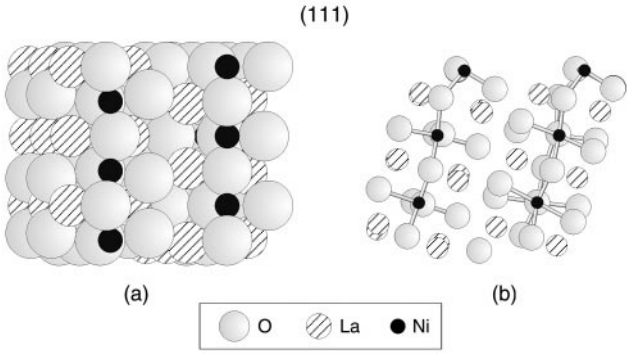

Fig. 7 Surface structures for the {111} surface of La_2NiO_4: (a) unrelaxed (top view), (b) relaxed (side view). For clarity, the top and side views are shown with full and half scale ion radii, respectively.

displacements occur some 30 Å into the bulk. This surface rearrangement from the unrelaxed (perfect) configuration reduces the surface energy by 68%.

{001} Surface

Fig. 1(b) and Fig. 4 indicate that this surface is terminated by Ni and O ions. In a similar manner to the {100} surface, the strain is reduced by the surface layer relaxing outwards, away from the bulk. The Ni–O_{eq} bonds of the truncated surface octahedra are displaced as alternate oxygens move slightly towards and away from the surface.

{110} Surface

Fig. 1(c) and Fig. 5 show that this surface is terminated by all three ion species. Unlike the preceding facets, this surface relaxes by moving the majority of the surface atoms towards the bulk. There are minor displacements of complete NiO_6 octahedra, although their neighbouring La ions descend towards the bulk by 0.3 Å. However, the equatorial oxygens of the truncated octahedra relax towards the bulk (0.5 Å). This overall relaxation reduces the {110} surface energy by 62% and creates a 'rumpling' effect of the outermost surface layer.

{011} Surface

Fig. 1(d) and Fig. 6 show that this surface is terminated by La and O species. Relaxation is achieved by surface atom displacement away from the bulk. La and O ions move outwards (0.9 and 1.2 Å, respectively) from the surface octahedra. Similar patterns of relaxation are experienced several layers down as the octahedra rearrange to minimise the effects felt from the surface reconstruction. A sinusoidal 'buckling' of the Ni–O_{eq} planes occurs as they descend into the bulk.

{111} Surface

Fig. 1(e) and Fig. 7 show that this surface is terminated by a nickel oxide layer of incomplete octahedra. The surface ions relax towards the bulk in order to reduce surface strain, with a decrease of the surface energy by 66%. In a similar manner to the incomplete NiO_6 octahedra exposed on the {110} surface, the largest displacements are those of the axial oxygens which contract towards the bulk by 0.8 Å. This causes a sinusoidal buckling of the Ni–O_{eq} layers.

In general, Figs. 3–7 show how the surfaces of La_2NiO_4 feature rumpling effects, in common with those that contain more than one type of atom. Similarly, rumpling of both the {100} and OLa {001} surfaces of the isostructural La_2CuO_4 crystal has also been predicted.[39] The structural effects of surface facetting and of surface concentrations of Ni(III) holes are subjects for further investigation.

Surface energies and morphologies from transition metal substitution

Previous studies of the bulk structure[28] of La_2NiO_4 indicate that on partial replacement of nickel by transition metal ions, Ni(III) hole formation is enhanced by Fe substitution but is less favourable for Cu addition. This correlates well with the catalytic performance for hypochlorite decomposition in which experimental studies show that 25% replacement of Ni by Fe leads to an increase in catalytic activity, but is reduced if Cu is the dopant.[10] Before defect calculations are considered at the surface, the surface structures of $La_2Ni_{0.75}M_{0.25}O_4$ (M = Fe,Cu) were modelled.

Fig. 8 plots the relaxed surface energies of the solid solutions $La_2Ni_{0.75}M_{0.25}O_4$ (where M = Fe, Cu and Ni (undoped)). In general, both dopants reduce the surface energies by varying degrees. More specifically, Fe substitution reduces the energy of the {100} surface to a greater extent than Cu addition. Interestingly, Fe reduces the surface energy of {011} whereas Cu increases the energy relative to undoped La_2NiO_4. Although the order of surface energies differs from pure La_2NiO_4, {100} and {111} are still the two most stable surfaces in the doped systems.

Previous studies have found that the growth of crystals in the presence of foreign ions can greatly influence the crystal morphology. The surface energies for $La_2Ni_{0.75}M_{0.25}O_4$ were therefore utilised to generate morphologies, shown schematically in Fig. 9. The percentage change in area of each surface relative to pure La_2NiO_4 is also plotted for the two solid solutions (Fig. 10). In contrast to the undoped system, both dopants are predicted to cause {100} to be the major surface of the morphology instead of {111}. Fig. 10 shows that both cation additions increase the coverage of {100} by ~15% and decrease the {111} coverage by ~25%. Both dopants increase the expression of the {001} surface but Cu to a greater extent than Fe. Overall, the morphologies are similar with a slightly more elongated habit for the Fe doped system. However, a key difference is that the {011} face appears in the Fe system, but is not expressed in either the Cu doped or undoped crystal.

Defects and Sr doping at surfaces

The simulation approach to aliovalent doping is based on assessing the energetics of dissolution and the nature of the charge-compensating defects. Focusing on Sr^{2+} as the commonly used acceptor dopant in La_2NiO_4, the charge compensation mechanisms can be represented by two defect

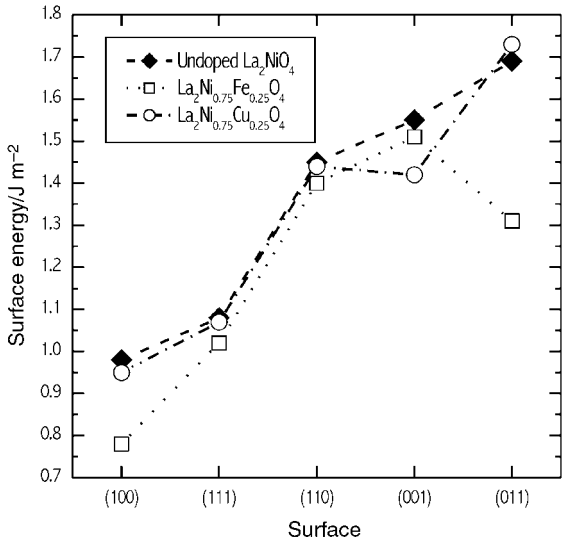

Fig. 8 Plot of surface energies for La_2NiO_4 (undoped), $La_2Ni_{0.75}Fe_{0.25}O_4$ and $La_2Ni_{0.75}Cu_{0.25}O_4$ (lines are guide to the eye).

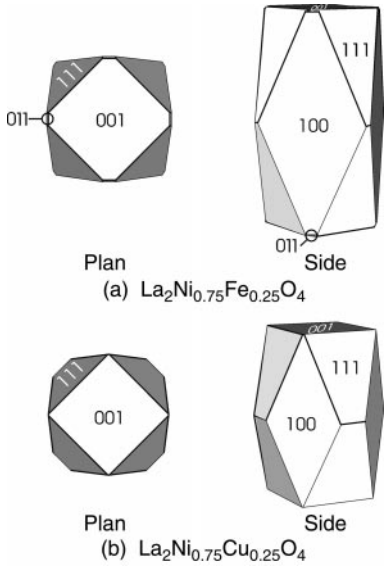

Fig. 9 Calculated crystal morphologies: (a) $La_2Ni_{0.75}Fe_{0.25}O_4$, (b) $La_2Ni_{0.75}Cu_{0.25}O_4$.

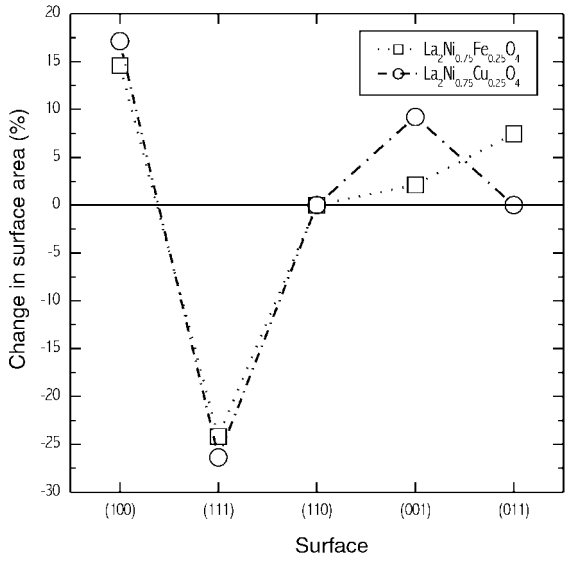

Fig. 10 Change in surface area of the single crystal on isovalent doping of La_2NiO_4 with Fe and Cu (normalised to undoped La_2NiO_4).

equations involving either oxygen vacancy ($V_O^{\cdot\cdot}$) or hole ($h^{\cdot}$) formation:

$$2SrO + 2La_{La}^{\times} + O_O^{\times} \rightleftarrows 2Sr_{La}^{/} + V_O^{\cdot\cdot} + La_2O_{3(surf)} \quad (2)$$

$$2SrO + 2La_{La}^{\times} + 1/2O_2 \rightleftarrows 2Sr_{La}^{/} + 2h^{\cdot} + La_2O_{3(surf)} \quad (3)$$

where $Sr_{La}^{/}$ signifies the dopant substitutional. The energies of solution were evaluated by combining appropriate defect and cohesive energy terms. The positive holes are treated in localised terms as Ni^{3+} and O^{-} small polaron species. Our studies have favoured nickel holes over oxygen holes although we acknowledge that the question of whether such species are predominantly Ni 3d or O 2p character remains unclear and would require the use of quantum mechanical methods. Nevertheless, calculations of this type have a crucial role in unravelling the nature of the defect processes responsible for the redox chemistry.

The METADISE code[22] is used to calculate the defect energies of single point defects and neutral defect clusters on the relaxed surfaces of La_2NiO_4. Various geometries exist for the defect clusters, so that for each surface there are several sites in which the defect and the Sr substitutional can be placed. Each possibility was examined with the lowest energy configuration selected.

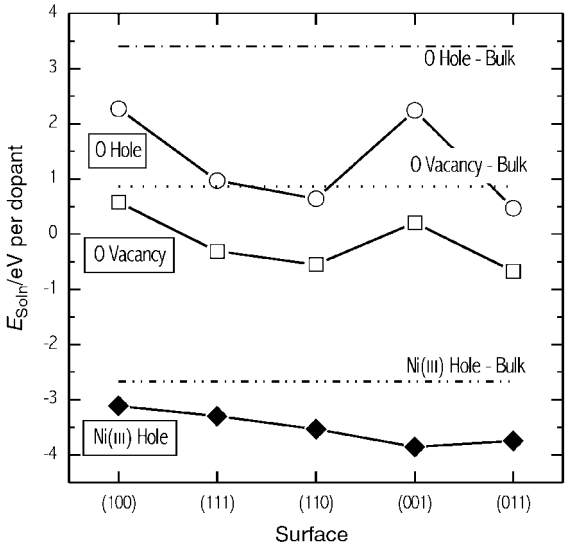

Fig. 11 Solution energies for Sr^{2+} doping of La_2NiO_4 at each low index surface with three charge-compensation mechanisms. Bulk values are also indicated.

The solution energies for Sr incorporation (calculated using eqns. (2) and (3)) are displayed in Fig. 11. Two main points emerge. First, as found from our previous bulk calculations[28] the most favourable mechanism is that of Ni(III) hole formation. This is consistent with spectroscopic studies[7,8,47] of the valence band density of states which find that holes are created by Sr doping in La_2NiO_4. It is believed that higher valence Ni is correlated to the catalytic activity of these nickelates. Indeed, the role of Ni(III) species as active sites in nickelate perovskites is well established in other catalytic studies of, for example, the oxidation of NH_3.[5,48] Kharton *et al.*[17] also show that the electronic conductivity of solid solutions based on doped La_2NiO_4 increases with increasing Sr content. Second, Fig. 11 reveals that the solution energy *via* all three mechanisms is lower at the surface than in the bulk. This suggests that it is favourable for these defects to 'segregate' to these surfaces. Indeed high resolution ESCA studies of $La_{2-x}Sr_xNi_{1-y}Fe_yO_{4+\delta}$ show segregation of Sr leading to Sr-rich surface regions.[8] This phenomenon is also consistent with behaviour seen in the related oxide $La_{2-x}Sr_xCuO_4$.[39]

From the catalytic viewpoint the {111}, {100} and {001} faces are predicted to dominate the equilibrium morphology, of which {001} and {011} have the most favourable Sr solution energy to form Ni(III). Interestingly, Fe doping increases the expression of these two surfaces to the crystal morphology, hence increasing the surface area of these faces for catalytic reactions. Previous bulk simulations find that on Sr doping of the solid solutions $La_2Ni_{0.75}M_{0.25}O_4$ (M = Mn,Fe,Co,Cu), both Mn and Fe enhance Ni^{3+} hole formation which would promote overall reactivity of the catalyst material and increase p-type conductivity. These results accord well with observation in which Fe incorporation improves the catalytic performance whereas Cu doping depresses the activity.

Conclusions

Computer modelling methods have been used to investigate the defect and surface structural properties of pure and doped La_2NiO_4. These aspects are of relevance to their potential use in catalysis, SOFCs and ceramic membranes, and to the

behaviour of nanoparticles. The following main features emerge from the results.

(1) Relaxed surface energies were calculated for low index surfaces of La_2NiO_4. The simulations reveal substantial "rumpling-type" surface relaxation at the atomic level. The equilibrium crystal morphology is predicted to be anisotropic with a tetragonal-like habit. The {111}, {100} and {001} surfaces dominate the morphology in the absence of water or surface irregularities, and are therefore expected to play a role in catalysis and inter-granular conductivity. The {111} and {001} surfaces are terminated by both Ni^{2+} and O^{2-} ions, whereas {100} terminates with O^{2-} ions.

(2) Partial substitution of the Ni site by Fe and Cu with composition $La_2Ni_{0.75}M_{0.25}O_4$ was simulated. The crystal morphologies are similar to pure La_2NiO_4 with a slightly more elongated habit for the Fe doped system. However, a small difference is that the {011} face appears in the Fe system, but is not expressed in either the Cu doped or undoped crystal.

(3) Strontium substitution of the La site is calculated to be favourable with the formation of Ni(III) holes in accord with spectroscopic studies of the valence band density of states. This is consistent with bulk simulations and catalytic models in which an increasing nickel oxidation state (Ni(III) species) is correlated to the observed catalytic activity and p-type conductivity.

(4) The lower defect energies at the surface relative to the bulk suggest a tendency for the segregation of Sr dopant ions to the outermost surface (which would lead to Sr-rich surface regions). This may have an effect on surface exchange and diffusion processes. Finally, it would be of interest to extend the present work to encompass surface simulations of the oxygen-excess material $La_2NiO_{4+\delta}$ comprised of oxygen interstitial defects.

Acknowledgements

This work was supported by an EPSRC/CASE studentship with Synetix (M. S. D. R.). The simulations were performed on the supercomputer facilities at the Rutherford Appleton Laboratory.

References

1 T. Tagawa and H. Imai, *J. Chem. Soc., Faraday Trans.*, 1988, **84**, 923.
2 A. K. Ladavos and P. J. Pomonis, *Appl. Catal. B*, 1993, 27.
3 J. Choisnet, N. Abadzhieva, P. Stefanov, D. Klissurski, J. M. Bassat, V. Rives and L. Minchev, *J. Chem. Soc., Faraday Trans.*, 1994, **90**, 1987.
4 T. R. Ling, Z. B. Chen and M. D. Lee, *Catal. Today*, 1995, **26**, 79.
5 Z. Yu, L. Gao, S. Yuan and Y. Wu, *J. Chem. Soc., Faraday Trans.*, 1992, **88**, 3245.
6 P. D. L. Mora, C. D. Teresa and L. Vicente, *Mater. Res. Soc. Symp. Proc.*, 1993, 331.
7 W. R. Flavell, J. Hollingworth, J. F. Howlett, A. G. Thomas, M. Sarker, S. Squire, Z. Hashim, M. Mian, P. L. Wincott, D. Teehan, S. Downes and F. E. Hancock, *J. Synchrotron Radiat.*, 1995, **2**, 264.
8 J. F. Howlett, W. R. Flavell, A. G. Thomas, J. Hollingworth, S. Warren, Z. Hashim, M. Mian, S. Squire, H. R. Aghabozorg, M. M. Sarker, P. L. Wincott, D. Teeham, S. Downes, D. S. Law and F. E. Hancock, *Faraday Discuss.*, 1996, **105**, 337.
9 J. Hollingworth, W. R. Flavell, A. G. Thomas, S. C. Grice, C. E. J. Mitchell, P. M. Dunwoody, S. Warren, S. J. Squire, P. G. D. Marr, S. W. Downes and F. E. Hancock, *J. Electron Spectrosc. Relat. Phenom.*, 1999, **103**, 765.
10 F. King and F. E. Hancock, *Catal. Today*, 1996, **27**, 203.
11 R. J. Cava, B. Batlogg, T. T. M. Palstra, J. J. Krajewski, W. F. Peck, A. P. Ramirez and L. W. Rupp, *Phys. Rev. B*, 1991, **43**, 1229.
12 K. Sreedhar and J. M. Honig, *J. Solid State Chem.*, 1994, **111**, 147.
13 S. H. Lee and S. W. Cheong, *Phys. Rev. Lett.*, 1997, **79**, 2514; A. Villesuzanne, A. Demourgues, J. C. Grenier, J. P. Doumerc, A. Wattiaux and M. Pouchard, *J. Mater. Chem.*, 1997, **7**, 953.
14 J. E. Millburn, M. A. Green, D. A. Neumann and M. J. Rosseinsky, *J. Solid State Chem.*, 1999, **145**, 401.
15 V. Vashook, N. Trofimenko, H. Ullmann and L. Makhnach, *Solid State Ionics*, 2000, **131**, 329.
16 V. V. Vashook, I. I. Yushkevich, L. V. Kokhanovsky, L. V. Makhnach, S. P. Tolochko, I. F. Kononyuk, H. Ullmann and H. Altenburg, *Solid State Ionics*, 1999, **119**, 23.
17 V. V. Kharton, A. P. Viskup, E. N. Naumovich and F. M. B. Marques, *J. Mater. Chem.*, 1999, **9**, 2623.
18 S. J. Skinner and J. A. Kilner, *Solid State Ionics*, 2000, **135**, 709.
19 P. J. Gellings and H. J. M. Boumeester, *Catal. Today*, 2000, **58**, 1.
20 C. R. A. Catlow, in *Computer-Aided Molecular Design*, ed. W. G. Richards, IBC Technical Services, London, 1989, ch. 21.
21 A. K. Cheetham and P. Day, *Solid State Chemistry Techniques*, Clarendon Press, Oxford, 1987, ch. 7.
22 G. W. Watson, E. T. Kelsey, N. H. de Leeuw, D. J. Harris and S. C. Parker, *J. Chem. Soc., Faraday Trans.*, 1996, **92**, 433.
23 S. D. Loades, S. W. Carr, D. H. Gay and A. L. Rohl, *J. Chem. Soc., Chem. Commun.*, 1994, **11**, 1369.
24 M. S. Islam, D. J. Ilett and S. C. Parker, *J. Phys. Chem.*, 1994, **98**, 9637.
25 P. M. Oliver, G. W. Watson, E. T. Kelsey and S. C. Parker, *J. Mater. Chem.*, 1997, **7**, 563.
26 M. S. Islam, *J. Mater. Chem.*, 2000, **10**, 1027.
27 M. S. Islam, M. S. D. Read and S. D'Arco, *Faraday Discuss.*, 1997, **106**, 367.
28 M. S. D. Read, M. S. Islam, F. King and F. E. Hancock, *J. Phys. Chem. B*, 1999, **103**, 1558.
29 L. Minervini, R. W. Grimes, J. A. Kilner and K. E. Sickafus, *J. Mater. Chem.*, 2000, **10**, 2349.
30 M. J. Davies, S. C. Parker and G. W. Watson, *J. Mater. Chem.*, 1994, **4**, 813.
31 G. Balducci, J. Kašpar, P. Fornasiero, M. Graziani, M. S. Islam and J. D. Gale, *J. Phys. Chem. B*, 1998, **102**, 557.
32 M. S. D. Read, M. S. Islam, G. W. Watson, F. King and F. E. Hancock, *J. Mater. Chem.*, 2000, **10**, 2298.
33 D. E. Parry, *Surf. Sci.*, 1975, **49**, 433.
34 D. E. Parry, *Surf. Sci.*, 1976, **54**, 195.
35 F. Bertaut, *C. R. Hebd. Seances Acad. Sci.*, 1958, **246**, 3447.
36 P. W. Tasker, *J. Phys. C: Solid State Phys.*, 1979, **12**, 4977.
37 G. Wulff, *Z. Kristallogr. Kristallgeom.*, 1901, **39**, 449.
38 J. W. Gibbs, *On the Equilibrium of Heterogeneous Substances*, Longman, New York, vol. 1, 1928.
39 P. R. Kenway, S. C. Parker and W. C. Mackrodt, *Surf. Sci.*, 1995, **326**, 301.
40 W. C. Mackrodt, *J. Chem. Soc., Faraday Trans.*, 1989, **85**, 541.
41 N. L. Allan, P. Kenway, W. C. Mackrodt and S. C. Parker, *J. Phys. B: Condens. Matter*, 1989, **1**, SB119.
42 J. O. Titiloye, S. C. Parker, D. J. Osguthorpe and S. Mann, *J. Chem. Soc., Chem. Commun.*, 1991, 1494.
43 D. Scarano, G. Ricchiardi, S. Bordiga, P. Galletto, C. Lamberti, G. Spoto and A. Zecchina, *Faraday Discuss.*, 1996, **105**, 119.
44 P. M. Oliver, G. W. Watson, E. T. Kelsey and S. C. Parker, *J. Mater. Chem.*, 1997, **7**, 563.
45 S. C. Parker, P. M. Oliver, N. H. DeLeeuw, J. O. Titiloye and G. W. Watson, *Phase Transitions*, 1996, **61**, 83.
46 W. J. Jang and H. Takei, *Jpn. J. Appl. Phys.*, 1991, **30**, 251.
47 Z. Tan, S. M. Heald, S. W. Cheong, A. S. Cooper and A. R. Moodenbaugh, *Phys. Rev. B*, 1993, **47**, 12365.
48 S. Ramesh, S. S. Manoharan, M. S. Hegde and K. C. Patil, *J. Catal.*, 1995, **157**, 749.